

Cross-modal Full-mode Fine-grained Alignment for Text-to-Image Person Retrieval

HAO YIN and XIN MAN, Shenzhen Institute for Advanced Study, University of Electronic Science and Technology of China, China

FEIYU CHEN, JIE SHAO*, and HENG TAO SHEN, University of Electronic Science and Technology of China, China Sichuan Artificial Intelligence Research Institute, China

Text-to-Image Person Retrieval (TIPR) is a cross-modal matching task designed to identify the person images that best correspond to a given textual description. The key difficulty in TIPR is to realize robust correspondence between the textual and visual modalities within a unified latent representation space. To address this challenge, prior approaches incorporate attention mechanisms for implicit cross-modal local alignment. However, they lack the ability to verify whether all local features are correctly aligned. Moreover, existing methods tend to emphasize the utilization of hard negative samples during model optimization to strengthen discrimination between positive and negative pairs, often neglecting incorrectly matched positive pairs. To mitigate these problems, we propose FMFA, a cross-modal Full-Mode Fine-grained Alignment framework, which enhances global matching through explicit fine-grained alignment and existing implicit relational reasoning—hence the term “full-mode”—without introducing extra supervisory signals. In particular, we propose an Adaptive Similarity Distribution Matching (A-SDM) module to rectify unmatched positive sample pairs. A-SDM adaptively pulls the unmatched positive pairs closer in the joint embedding space, thereby achieving more precise global alignment. Additionally, we introduce an Explicit Fine-grained Alignment (EFA) module, which makes up for the lack of verification capability of implicit relational reasoning. EFA strengthens explicit cross-modal fine-grained interactions by sparsifying the similarity matrix and employs a hard coding method for local alignment. We evaluate our method on three public datasets, where it attains state-of-the-art results among all global matching methods. The code for our method is publicly accessible at <https://github.com/yinhao1102/FMFA>.

CCS Concepts: • **Information systems** → **Image search**; • **Computing methodologies** → *Object identification*.

Additional Key Words and Phrases: Cross-modal retrieval, Person search, Fine-grained alignment

ACM Reference Format:

Hao Yin, Xin Man, Feiyu Chen, Jie Shao, and Heng Tao Shen. 2025. Cross-modal Full-mode Fine-grained Alignment for Text-to-Image Person Retrieval. *ACM Trans. Multimedia Comput. Commun. Appl.* 1, 1, Article 1 (January 2025), 22 pages. <https://doi.org/10.1145/3786798>

*Corresponding author.

Authors' Contact Information: Hao Yin, yinhao1102@std.uestc.edu.cn; Xin Man, manxin@std.uestc.edu.cn, Shenzhen Institute for Advanced Study, University of Electronic Science and Technology of China, Shenzhen, China; Feiyu Chen, chenfeiyu@uestc.edu.cn; Jie Shao, shaojie@uestc.edu.cn; Heng Tao Shen, shenhengtao@hotmail.com, University of Electronic Science and Technology of China, Chengdu, China and Sichuan Artificial Intelligence Research Institute, Yibin, China.

Permission to make digital or hard copies of all or part of this work for personal or classroom use is granted without fee provided that copies are not made or distributed for profit or commercial advantage and that copies bear this notice and the full citation on the first page. Copyrights for components of this work owned by others than the author(s) must be honored. Abstracting with credit is permitted. To copy otherwise, or republish, to post on servers or to redistribute to lists, requires prior specific permission and/or a fee. Request permissions from permissions@acm.org.

© 2025 Copyright held by the owner/author(s). Publication rights licensed to ACM.

ACM 1551-6865/2025/1-ART1

<https://doi.org/10.1145/3786798>

1 Introduction

Text-to-Image Person Retrieval (TIPR) seeks to understand natural language descriptions and identify the most relevant person image within a large gallery [31]. Unlike general image-text retrieval [5, 6, 44, 47, 50], which tends to achieve semantic-based matching between text and image, TIPR is specifically designed for identifying individuals. TIPR requires the accurate modeling of fine-grained correspondences between textual and visual modalities, owing to the large intra-class variance and small inter-class difference. This substantial intra-class variation arises from two aspects: (1) visual appearances of the same identity exhibit dramatic variations under different poses, viewpoints, and illumination conditions, and (2) textual descriptions are influenced by differences in phrasing, word order and textual ambiguities. Therefore, the primary challenges in TIPR are how to extract discriminative global representations from image-text pairs and how to achieve precise cross-modal fine-grained alignment. Existing methods for tackling these challenges can be roughly divided into two main categories: global matching methods and local matching methods.

Some global matching methods [58, 59] obtain discriminative global representations by aligning images and texts, which are projected into a joint embedding space. Their widely adopted loss functions include the Cross-Modal Projection Matching (CMPM) loss [58] and the Similarity Distribution Matching (SDM) loss [21]. The CMPM loss highlights the gap between the scalar projections of image-text pairs and their matched label indicators. In comparison, the SDM loss boosts global matching performance by minimizing the Kullback-Leibler (KL) divergence between the normalized similarity profile of image-text pairs and the true label distribution. In addition, the SDM loss incorporates a temperature hyperparameter to make model updates concentrate on hard negative samples, yet it leads to the neglect of unmatched positive pairs, as shown in Figure 1a. However, in TIPR, the accurate matching of positive pairs is prioritized over merely distinguishing between positive and negative pairs. Meanwhile, some local matching methods [2, 11, 35] incorporate attention mechanisms to achieve cross-modal fine-grained alignment. For instance, RaSa [2] constructs a cross-modal encoder to generate multimodal representations for subsequent fine-grained alignment. Building on RaSa, MARS [11] integrates a Masked AutoEncoder (MAE) decoder [14] to reconstruct masked image patch sequences into their original unmasked form, thereby facilitating cross-modal fine-grained alignment. However, these methods rely on attention mechanisms to implicitly aggregate local image-text representations. As a result, they yield only the final multimodal representation, without revealing the details of the aggregation process. Consequently, these implicit aggregation methods make it difficult to determine whether the aggregated multimodal representations correctly encode the corresponding visual and textual information.

To remedy these concerns, we propose **FMFA**, a **cross-modal Full-Mode Fine-grained Alignment framework**, which enhances global matching through full-mode fine-grained alignment, including explicit fine-grained image-text alignment and existing implicit relational reasoning. Specifically, we design an **Adaptive Similarity Distribution Matching (A-SDM)** module to ensure the correct matching of positive image-text pairs. Within the joint embedding space, the A-SDM module adaptively pulls positive pairs closer together. In cases of mismatched positive pairs, the A-SDM module adaptively regulates the pulling force based on their relative distance within the joint embedding space, as shown in Figure 1b, thus improving cross-modal global alignment. Based on the insight that each word in a caption can be associated with several image patches [3], we introduce an **Explicit Fine-Grained Alignment (EFA)** module. The EFA module derives multimodal representations through explicit aggregation with a sparse similarity matrix. During this process, the sparse similarity matrix between text and image reflects the contribution of textual and visual representations to the final multimodal representation. To minimize redundancy and reduce

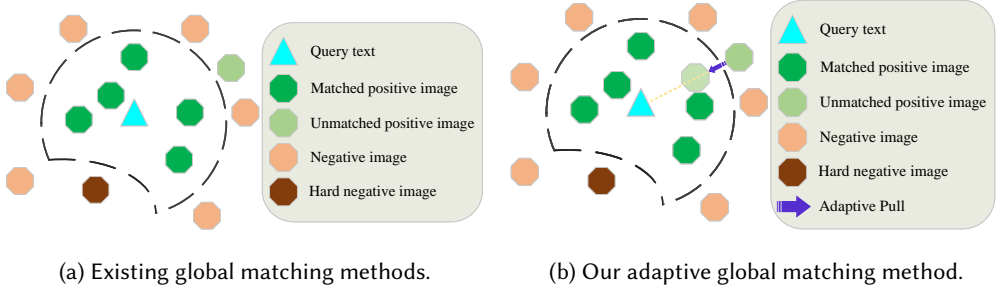


Fig. 1. Evolution of global matching methods for text-to-image person retrieval. (a) Existing global matching methods focus on hard negative samples to learn a discriminative boundary in a common latent space, thus enhancing the distinction between positive and negative samples. (b) Our adaptive global matching method builds on a discriminative boundary and concentrates on unmatched positive samples, adaptively pulling them closer to the corresponding query text.

the computational cost during training, the EFA module employs hard coding alignment between the aggregated multimodal representation and its original visual and textual representations. These designs allow EFA to realize fine-grained cross-modal interactions and assist the backbone network in learning more distinctive global image-text representations without introducing additional supervision. FMFA is evaluated on three public benchmarks [10, 27, 60], and it attains competitive top-level performance along with high inference efficiency. We highlight our key contributions below:

- We introduce FMFA to explicitly leverage fine-grained interactions for improving cross-modal alignment, without incurring extra supervision or inference overhead.
- We present an adaptive similarity distribution matching module aimed at precisely aligning image-text pairs in a shared embedding space. It adaptively adjusts to narrow the distance between mismatched positive pairs, ensuring more precise matching.
- We develop an explicit fine-grained alignment module, which leverages the sparse similarity matrix for explicit aggregation and employs a hard coding method in cross-modal fine-grained alignment to minimize redundant information.

2 Related Work

Text-to-Image Person Retrieval (TIPR) was initially proposed by Li et al. [27], who created the CUHK-PEDES dataset. Unlike visual-based person retrieval [7, 8, 16, 56], the core challenge of TIPR lies in constructing a shared latent space that enables coherent alignment between visual and textual representations. Existing methods can be typically classified into global and local matching approaches.

Early global methods [59, 60] directly aligned the global representations of images and text in a joint embedding space. Schroff et al. [39] proposed a triplet ranking loss to enforce a margin constraint between positive and negative pairs, and Zhang et al. [58] introduced the CMPM/C loss to minimize the discrepancy between the scalar projection of image-text pairs and their labels. However, these global methods lack cross-modal fine-grained interactions, which restrict their ability to capture detailed semantic correspondences. To address this limitation, early local matching methods [12, 42, 49] explicitly aligned local visual and textual features to achieve fine-grained cross-modal interactions. Nevertheless, they rely on unimodal pre-trained models (e.g., BERT [9]

and ResNet [15]), failing to exploit the strong cross-modal alignment capability of recent pre-trained Vision-Language Models (VLMs) [25, 26, 53].

Recent local matching methods [11, 19, 32, 36, 52] have benefited greatly from VLMs and introduced VLMs to enhance cross-modal alignment. Park et al. [35] utilized a modified Contrastive Language-Image Pre-training (CLIP) [37] model as the feature extractor and designed a slot attention-based [30] part discovery module to identify discriminative human parts without extra supervision, while Bai et al. [2] used the align-before-fuse model [26] as the backbone and introduced a cross-modal encoder for fine-grained alignment. Although effective, these methods involve complex computations during inference, leading to high time and memory costs, which limit their applicability to real-time systems.

On another line of research, several studies [41, 45, 55] have explored leveraging large-scale image-text pairs in the person Re-IDentification (ReID) domain to VLMs. Zuo et al. [61] utilized CUHK-PEDES and ICFG-PEDES to train an image captioner, aiming to generate comprehensive textual descriptions for pedestrian images. Yang et al. [55] employed BLIP-2 [24] to produce attribute-aware captions for diffusion-generated pedestrian images [38], while Jiang et al. [22] leveraged recent Multi-modal Large Language Models (MLLMs), such as Qwen-VL [1] and LLaVA [28], to automatically annotate large-scale ReID datasets in a human-like manner. The CLIP models pre-trained on large-scale ReID datasets exhibit strong zero-shot performance. Their compatibility with global matching methods—which relies solely on global features and has a simple inference pipeline—makes them particularly suitable for direct fine-tuning in such settings.

Recent global matching methods [17, 21, 43] have integrated local fine-grained alignment modules into global matching frameworks to obtain more discriminative global representations. Shu et al. [43] introduced a bidirectional mask modeling mechanism that randomly masks image patches and text words, encouraging the model to infer missing semantics and implicitly learn local visual-textual correspondences. He et al. [17] proposed the Vision-Guided Semantic-Group (VGSG) network to cluster textual tokens into semantic groups and align them with corresponding visual regions under the guidance of vision features, achieving group-level fine-grained alignment within a global representation space. Similarly, Jiang et al. [21] developed IRRA to employ an Implicit Relation Reasoning (IRR) module based on attention mechanisms to capture latent cross-modal relations, enhancing global alignment. Although these methods enhance fine-grained cross-modal interactions within global matching frameworks, their implicit or group-level alignment strategies may still fail to guarantee precise local correspondences. In light of these limitations, we propose FMFA, which aims to enhance the global matching ability of the model by achieving cross-modal full-mode fine-grained alignment, including explicit fine-grained alignment and implicit relation reasoning.

3 Method

This section introduces the proposed FMFA framework. Figure 2 presents an overview of FMFA, and further details of the framework are elaborated in the subsequent subsections.

3.1 Feature Extraction

Motivated by the success of IRRA [21], we use the modified full CLIP [37] visual and textual encoders to enhance cross-modal alignment capabilities while reducing inference costs.

Visual Modality. Given an input image $I \in \mathbb{R}^{H \times W \times C}$, we employ a CLIP-pretrained Vision Transformer (ViT) to attain its image representation. An image is first divided into $N = H \times W / P^2$ distinct patches of size $P \times P$, which are then transformed into one-dimensional token embeddings $\{f_i^v\}_{i=1}^N$ via a learnable linear projection. After adding positional encodings and a [CLS] token, the sequence $\{f_{cls}^v, f_1^v, \dots, f_N^v\}$ is passed through L transformer layers to capture dependencies

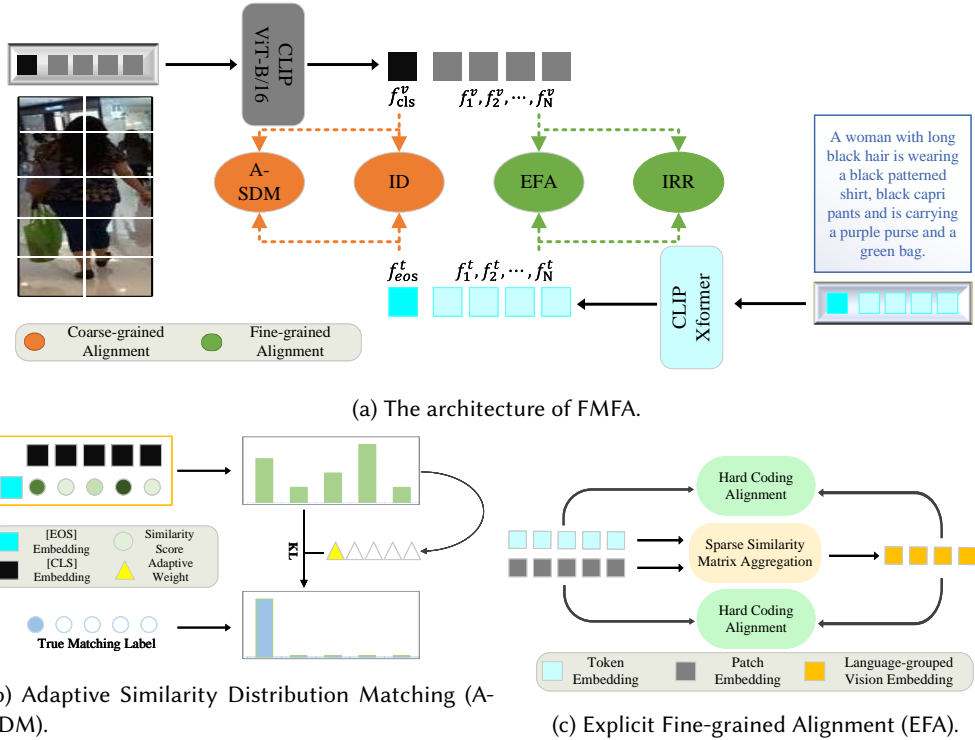


Fig. 2. The illustration of our FMFA framework. (a) Our FMFA contains a two-stream feature extraction network and four distinct modules for structured representation learning, namely Identity Identification (ID loss), Adaptive Similarity Distribution Matching (A-SDM), Explicit Fine-grained Alignment (EFA) and Implicit Relation Reasoning (IRR). The former two are coarse-grained alignment modules and the latter two are fine-grained alignment modules. Modules linked via dashed connections are omitted during inference. (b) A-SDM obtains the adaptive weight through the similarity score of unmatched positive pairs, adaptively pulling positive pairs closer and dynamically adjusting the pulling force. (c) EFA achieves fine-grained interaction by hard coding alignment of token or patch embeddings and their corresponding language-grouped vision embedding, which is derived from an aggregated sparse similarity matrix.

among patches. Finally, the [CLS] token embedding f_{cls}^v is linearly mapped into the joint image-text embedding space, producing the compact global feature of the image.

Textual Modality. Given an input text T , we utilize the CLIP-Xformer textual extractor [37] to obtain its embedding. The text is first tokenized through lower-cased Byte Pair Encoding (BPE) [40] and framed with [SOS] and [EOS] tokens to indicate sequence boundaries. The resulting token sequence $\{f_{sos}^t, f_1^t, \dots, f_{eos}^t\}$ is processed by the transformer encoder, which models dependencies among tokens via masked self-attention. Finally, the [EOS] token embedding from the top layer, f_{eos}^t , is linearly mapped into the joint image-text representation space, generating a compressed global textual representation.

3.2 Adaptive Similarity Distribution Matching

Adopted from IRRA [21], we introduce a novel Adaptive Similarity Distribution Matching (A-SDM) module, which aims to adaptively pull the unmatched positive image-text pairs into a shared representation space, further enhancing the cross-modal global matching capability of the model.

Let the mini-batch contain B image-text pairs, we pair each text embedding g_i^t with its global image embedding g_j^v to form the set $\{(g_i^t, g_j^v), y_{i,j}\}_{j=1}^B$, where $y_{i,j}$ serves as the matching indicator. Specifically, $y_{i,j} = 1$ denotes a matched pair, while $y_{i,j} = 0$ denotes an mismatched pair. Let $\cos(\mathbf{a}, \mathbf{c}) = \mathbf{a}^\top \mathbf{c} / \|\mathbf{a}\| \|\mathbf{c}\|$ denotes the similarity of \mathbf{a} and \mathbf{c} . Subsequently, like SDM [21], the similarity matrix of image-text pairs is obtained through the following softmax function:

$$p_{i,j} = \frac{\exp(\cos(g_i^t, g_j^v) / \tau_1)}{\sum_{k=1}^B \exp(\cos(g_i^t, g_k^v) / \tau_1)}, \quad (1)$$

where τ_1 acts as a temperature term that modulates the spread of the resulting distribution. The probability $p_{i,j}$ quantifies how much the similarity between the text embedding g_i^t and the image embedding g_j^v contributes relative to the sum of all similarities between g_i^t and every image embedding in the mini-batch.

Let the i -th text T_i from the batch be designated as the query text and I_i be the corresponding image for T_i at rank- k , where $k > 1$. Different from IRRA [21], we propose to derive an adaptive weighting factor by assessing the similarity between the query text T_i and all image representations:

$$w_i^{t2i} = \alpha \cdot \left[\max_k p_{i,k} - p_{i,i} \right] + 1, \quad (2)$$

where α is a weight factor reflecting the contribution of unmatched image-text pairs to the cross-modal global matching ability of the model. Here, $\max_k p_{i,k}$ indicates the top similarity value between the text T_i and every image within the mini-batch, while $p_{i,i}$ refers to the similarity associated with its corresponding positive image. The constant term “+1” ensures that when T_i and its corresponding image I_i are correctly matched, the weight w_i^{t2i} defaults to 1. In this case, the A-SDM loss reduces to the SDM loss [21], preventing overemphasis on correctly matched pairs while allowing the model to focus adaptively on harder and misaligned pairs. Conversely, $w_i^{t2i} > 1$ indicates that T_i and I_i are unmatched, increasing their contribution to the loss to enhance global cross-modal alignment. The A-SDM loss for mapping text to image within a mini-batch is subsequently formulated as:

$$\mathcal{L}_{t2i} = W^{t2i} * KL(\mathbf{p}_i \| \mathbf{q}_i) = \frac{1}{B} \sum_{i=1}^B w_i^{t2i} \sum_{j=1}^B p_{i,j} \log \left(\frac{p_{i,j}}{q_{i,j} + \epsilon} \right), \quad (3)$$

where ϵ is a tiny offset added to safeguard the computation from unstable values, and $q_{i,j} = y_{i,j} / \sum_{k=1}^B$ denotes the ground-truth matching probability.

In a complementary manner, the A-SDM loss for the image-to-text branch \mathcal{L}_{i2t} is derived by swapping the roles of the text and image features. The bi-directional A-SDM loss is formulated as:

$$\mathcal{L}_{A-sdm} = \mathcal{L}_{i2t} + \mathcal{L}_{t2i}. \quad (4)$$

3.3 Explicit Fine-grained Alignment

To effectively leverage fine-grained information, it is necessary to narrow the underlying disparity between visual and textual modalities. Although many attention-based fine-grained alignment approaches have shown effectiveness by implicitly associating local regions in images with textual fragments, they provide no direct means to verify whether these localized correspondences are accurately aligned. We propose an explicit cross-modal aggregation approach that leverages the

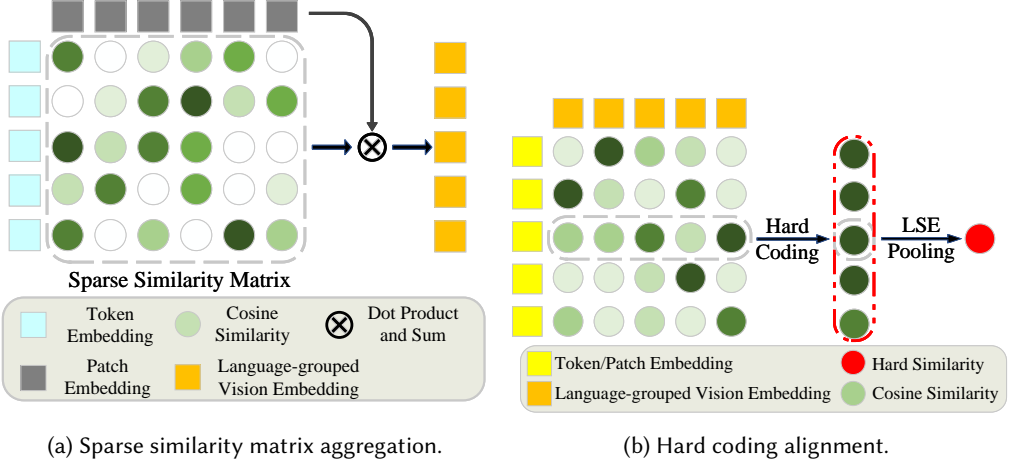


Fig. 3. Illustration of the EFA module. (a) EFA imposes a sparse structure on the similarity matrix relating token embeddings to patch embeddings, and obtains the language-grouped vision embeddings by aggregating the sparse similarity with its corresponding patch. (b) EFA obtains hard similarity through hard coding and LSE pooling, where the calculated hard similarity reflects the relationship between the language-grouped vision embeddings and their original token or patch embeddings.

sparse similarity matrix between the local image and text features. To further reduce redundant information and minimize memory and time costs during fine-grained alignment, we use hard coding to align the aggregated language-grouped vision embeddings with both image and text embeddings, as shown in Figure 2c.

Sparse Similarity Matrix Aggregation. Some methods [33, 57] incur substantial computational and memory overhead, as they evaluate pairwise relationships between every image patch and every text token, which limits scalability to large batch sizes. Therefore, we apply a sparsification strategy to reduce the full pairwise similarity computation. While softmax is commonly used for such sparse processing, it tends to produce low-entropy similarity distributions that impede effective gradient flow [18]. Thus, we further adopt a max-min normalization scheme to achieve a more stable and expressive sparse similarity aggregation.

An image I and its corresponding text T are encoded through the visual and textual encoders, respectively. As presented in Figure 3a, the similarity between image patches and text tokens is computed via the inner product of the last hidden states $\{f_i^t\}_{i=1}^L$ of the text transformer and $\{f_i^v\}_{i=1}^N$ of the vision transformer. $s_{i,j} = f_i^t \cdot f_j^v$ measures the similarity between the text token f_i^t and the image patch f_j^v , where \cdot denotes the inner product. To obtain the aggregation weight, each token i is first scaled to the range $[0,1]$ through the following min-max normalization:

$$\hat{s}_{i,j} = \frac{s_{i,j} - \min_k s_{i,k}}{\max_k s_{i,k} - \min_k s_{i,k}}. \quad (5)$$

We sparsify the normalized similarity matrix to encourage cross-modal interactions between each token and its patches with higher similarity:

$$\tilde{s}_{i,j} = \begin{cases} \hat{s}_{i,j} & \text{if } \hat{s}_{i,j} \geq \sigma \\ 0 & \text{otherwise} \end{cases}, \quad (6)$$

where σ is the sparsity threshold. σ is assigned the value $1/N$, where N corresponds to the total count of patches in the image. This ensures that each token has a minimum of one corresponding image patch for alignment. We compute the aggregation weights by:

$$agg_{i,j} = \frac{\tilde{s}_{i,j}}{\sum_{m=1}^M \tilde{s}_{i,j}}, \quad (7)$$

where M is the number of image patches retained with high similarity to the token i , and $agg_{i,j}$ quantifies the influence of patch j in forming the language-grouped vision embedding (referred to as joint embedding) associated with token i . This explicit aggregation strategy ensures a comprehensive interaction between token i and its corresponding patch j during local alignment. In particular, the aggregation weight $agg_{i,j}$ effectively captures the semantic relevance between token i and patch j , thereby facilitating precise alignment.

Next, we derive the corresponding joint embedding e_i as:

$$e_i = \sum_{j=1}^N agg_{i,j} \cdot f_j^v, \quad (8)$$

where N is the count of image patches. The resulting set of joint embedding e_i has the same length L as the text token f_i^t .

Hard Coding Alignment. We calculate the similarity between the joint embeddings $\{e_i\}_{i=1}^L$ and their corresponding original text embeddings $\{f_i^t\}_{i=1}^L$ as well as image embeddings $\{f_i^v\}_{i=1}^N$, respectively. To reduce both computational and memory costs, we adopt a hard coding similarity computation between the joint embeddings and their corresponding text and image embeddings, and the theoretical analysis of the hard coding is provided in Appendix A. For simplicity, we only present the calculation between the joint embeddings and the text embeddings, while the remaining computations follow a similar and symmetric approach.

For the text T and its corresponding joint embedding E , we calculate the original similarity matrix O between all text tokens $\{f_i^t\}_{i=1}^L$ and their joint embeddings $\{e_i\}_{i=1}^L$, where $o_{i,j} = f_i^t e_j^{\top} / \|f_i^t\| \|e_j\|$ means the cosine similarity of f_i^t and e_j . For the token f_i^t , we compute the weight factor between it and all joint embeddings using the following hard coding way:

$$\omega_{i,j} = \begin{cases} 1 & \text{if } j = \operatorname{argmax}_{j'=1 \cdots L} (o_{i,j'}) \\ 0 & \text{otherwise} \end{cases}. \quad (9)$$

Then, we utilize the LSE pooling [23] to compute the hard similarity between text T and its corresponding joint embedding E by:

$$\begin{aligned} hard_s(T, E) &= LSE - Pooling \left(\sum_{j=1}^L \omega_{i,j} o_{i,j} \right) \\ &= \frac{1}{\lambda} \log \sum_{i=1}^L \exp \left(\lambda \max_{j=1 \cdots L} o_{i,j} \right), \end{aligned} \quad (10)$$

where λ controls the degree to which the most relevant text embeddings and their corresponding joint embeddings are emphasized.

Given a batch containing B text embeddings along with their associated joint embeddings, we compute the hard coding similarity matrix $Hard_S$ following Eq. (9) and Eq. (10), as illustrated in Figure 3b. We calculate the EFA loss from the text to its joint embedding, adapted from the triplet

ranking loss [39]:

$$\mathcal{L}_{t2e} = \frac{1}{B} \log \sum_{\text{neg}} \exp \left(\frac{\text{Hard_}S_{\text{neg}} - \text{Hard_}S_{\text{pos}} + \text{margin}}{\tau_2} \right), \quad (11)$$

where τ_2 is a scaling factor adjusting the spread of the loss, and *margin* is a distance hyperparameter defining the minimal gap separating positive and negative pairs.

Similarly, the EFA loss from the joint embedding to its original text can be computed following Eq. (11), and we can calculate the EFA loss between image and its joint embedding through Eq. (9), Eq. (10) and Eq. (11). Then, we obtain a full EFA loss by:

$$\mathcal{L}_{efa} = \mathcal{L}_{t2e} + \mathcal{L}_{e2t} + \mathcal{L}_{i2e} + \mathcal{L}_{e2i}. \quad (12)$$

3.4 Training Objective

As mentioned, FMFA aims to improve both the global and local cross-modal alignment of image-text features within the shared embedding space. To realize this goal, the widely adopted ID loss [59] and IRR loss [21], together with the proposed EFA and A-SDM loss, are jointly utilized to train FMFA. The ID loss directly classifies the global features obtained from both the image and the text according to their identities, thereby enhancing the global alignment of the model. The IRR loss, based on the Masked Language Modeling (MLM) task [46], leverages an attention mechanism for implicit cross-modal interaction to obtain a joint embedding, and then predicts the [MASK] text token to enhance the local alignment of the model.

FMFA is trained end-to-end, with the complete training objective formulated as:

$$\mathcal{L} = \mathcal{L}_{id} + \mathcal{L}_{irr} + \mathcal{L}_{efa} + \mathcal{L}_{A\text{-}sdm}. \quad (13)$$

4 Experiments

4.1 Datasets and Settings

Datasets. We assess FMFA on three widely used text-based person retrieval datasets, following the data splits introduced in IRRA [21]. CUHK-PEDES [27] contains 40,206 images associated with 13,003 identities, where each image is paired with two textual descriptions. Of these identities, 11,003 are designated for training, while the remaining 1,000 identities are allocated separately to validation and test sets. ICFG-PEDES [10] includes 54,522 images belonging to 4,102 individuals, each image linked to a single sentence. The conventional setup utilizes 3,102 identities for training and reserves 1,000 identities for testing. RSTPReid [60] comprises 20,505 images from 4,101 identities captured across 15 camera views. Every identity corresponds to five images taken from different viewpoints, and each image is annotated with two descriptive captions. The dataset follows a split with 3,701 identities for training and 200 identities each for validation and testing.

Evaluation Metrics. To gauge retrieval quality, we primarily report Rank-K results ($K = 1, 5, 10$), which measure how often the correct item appears within the top-K predictions. Additionally, mean Average Precision (mAP) is adopted to summarize ranking accuracy over all query outcomes. In both cases, higher metric values correspond to superior model behavior.

Implementation Details. We utilize either the original CLIP model [37] or its ReID-domain pre-trained variants [22, 45] as encoders tailored to each modality. To maintain consistency, we employ the identical CLIP-ViT-B/16 model for visual encoding and Xformer for text encoding, following the setup used in IRRA [21] for our experiments. Specifically, images are resized to 384×128 pixels, and the maximum sequence length L for input word tokens is set to 77. The model is trained using the Adam optimizer for 60 epochs with a default cosine learning rate decay schedule, in contrast to the 100 epochs employed for the ICFG-PEDES dataset. The original CLIP model parameters are trained with an initial learning rate of $1e - 5$ and a batch size of 64. In particular,

Table 1. The margins utilized in the EFA loss. “T. to E.” means the EFA loss from textual embeddings to the corresponding joint embeddings, and “V. to E.” means the EFA loss from visual embeddings to the corresponding joint embeddings.

	CUHK-PEDES	ICFG-PEDES	RSTPReid
T. to E.	0.1	0.2	0.2
V. to E.	0.1	1.0	0.8

Table 2. The hardware configuration of our experimental environment.

Hardware	Details
CPU	Intel Xeon Gold 6330
GPU	NVIDIA RTX A6000
RAM	755 GB DDR4

the temperature τ_1 in the A-SDM loss is set to 0.02, while the temperature τ_2 in the EFA loss takes a value of 1.0. The weight factor α of A-SDM is set to 10.0 by default, and set to 1 in the RSTPReid dataset, and the factor λ in the LSE pooling is set to 1.0. Due to variations in data distribution, the margins used in the EFA loss differ across the three datasets. The specific margins used in Eq. (11) for each dataset are provided in Table 1. When using ReID-domain pre-trained CLIP models, we adopt the same initial learning rate and batch size as in NAM [45] and HAM [22], while keeping all other settings unchanged. The hardware configuration used in our experiments is shown in Table 2, while the detailed software environment is supplied in the code repository we have released.

4.2 Comparison with State-of-the-Art Methods

In this subsection, we provide a comparison with current state-of-the-art methods (e.g., NAM [45] and HAM [22]) on three public benchmark datasets. The methods are grouped into two types according to their underlying network architecture, as listed in Table 3, Table 4, and Table 5: those using VL-Backbones without ReID-domain pre-training and those incorporating ReID-domain pre-training. Furthermore, according to whether local features are utilized during inference, the baselines are further classified into local and global matching methods (denoted as “L” and “G” in the “Type” column, respectively). It should be noted that the baseline model presented in Table 3, Table 4, and Table 5 is referred to as IRRA^R, which represents the performance of our reimplementation of the IRRA model. CLIP means the ViT-B/16 architecture after fine-tuning under the InfoNCE loss [34].

Evaluation Results on CUHK-PEDES We measure the performance of FMFA on the CUHK-PEDES dataset, as presented in Table 3. When using the VL-Backbones without ReID-domain pre-training, FMFA achieves superior performance over advanced global matching methods, attaining 74.16% Rank-1 and 66.66% mAP, while surpassing IRRA by 0.74% in Rank-5 and 0.41% in Rank-10. When adopting the VL-Backbones with ReID-domain pre-training, FMFA maintains its superiority, and achieves Rank-5 accuracy exceeding 95% with the HAM-based backbone. Notably, FMFA with NAM-based backbone attains 91.33% in Rank-5, outperforming IRRA with the HAM-based backbone by 0.13%.

Evaluation Results on RSTPReid. We assess FMFA on the latest RSTPReid benchmark, as presented in Table 4. Using the VL-Backbones without ReID-domain pre-training, FMFA achieves competitive performance, attaining 61.05% Rank-1, 83.85% Rank-5, 89.80% Rank-10, and 48.22% mAP, respectively, outperforming IRRA by 1.55% in Rank-1 and 2.05% in Rank-5. When adopting

Table 3. Comparisons with state-of-the-art methods on the CUHK-PEDES dataset. “G”, “L” and “P” in the “Type” column stand for global-matching method, local-matching method and pre-trained model with ReID-domain respectively. “Image Enc.” and “Text Enc.” mean the backbone of image encoder and text encoder respectively. “IRRA^R” means the model that we reproduce.

Type	Method	Ref.	Image Enc.	Text Enc.	Rank-1	Rank-5	Rank-10	mAP
<i>VL-Backbones w/o ReID-domain pre-training:</i>								
G	LGUR [42]	MM22	ResNet50	BERT	65.25	83.12	89.00	-
	IVT [43]	ECCV22	ViT-B/16	BERT	65.59	83.11	89.21	-
	VGG [17]	TIP23	ResNet50	Transformer	67.52	84.37	90.26	-
	CLIP [37]	ICML21	CLIP-ViT	CLIP-Xformer	68.19	86.47	91.47	61.12
	DM-Adapter [29]	AAAI25	CLIP-ViT	CLIP-Xformer	72.17	88.74	92.85	64.33
	IRRA ^R [21]	CVPR23	CLIP-ViT	CLIP-Xformer	73.45	89.38	93.69	66.13
	TBPS-CLIP [4]	AAAI24	CLIP-ViT	CLIP-Xformer	73.54	88.19	92.35	65.38
	FMFA (ours)		CLIP-ViT	CLIP-Xformer	74.16	90.12	94.10	66.66
L	ACSA [20]	TMM22	Swin-B	BERT	63.56	81.49	87.70	-
	Han et al. [13]	arXiv21	CLIP-RN101	CLIP-Xformer	64.08	81.73	88.19	60.08
	PLOT [35]	ECCV24	CLIP-ViT	CLIP-Xformer	75.28	90.42	94.12	-
	RaSa [2]	IJCAI23	CLIP-ViT	BERT-base	76.51	90.29	94.25	69.38
	PTMI [32]	TIFS25	CLIP-ViT	CLIP-Xformer	76.02	89.93	94.14	70.85
	APTM [55]	MM23	Swin-B	BERT-base	76.53	90.04	94.15	66.91
	SCVD [51]	TCSTV24	CLIP-RN50	CLIP-Xformer	76.72	90.38	94.89	-
<i>VL-Backbones with ReID-domain pre-training:</i>								
P+G	UniPT [41] + IRRA [21]	ICCV23	CLIP-ViT	CLIP-Xformer	74.37	89.51	93.97	66.60
	PLIP [61] + IRRA [21]	NeurIPS24	CLIP-ViT	CLIP-Xformer	74.25	89.49	93.68	66.52
	NAM [45] + IRRA ^R	CVPR24	CLIP-ViT	CLIP-Xformer	76.67	91.11	94.60	68.42
	NAM [45] + FMFA (ours)		CLIP-ViT	CLIP-Xformer	77.23	91.33	94.75	68.53
	HAM [22] + IRRA ^R	CVPR25	CLIP-ViT	CLIP-Xformer	77.32	91.20	94.95	68.87
	HAM [22] + FMFA (ours)		CLIP-ViT	CLIP-Xformer	77.46	91.36	95.01	68.89

Table 4. Comparisons with state-of-the-art methods on the RSTPReid dataset.

Type	Method	Rank-1	Rank-5	Rank-10	mAP
<i>VL-Backbones w/o ReID-domain pre-training:</i>					
G	DSSL [60]	39.05	62.60	73.95	-
	IVT [43]	46.70	70.00	78.80	-
	CLIP [37]	54.05	80.70	88.00	43.41
	IRRA ^R [21]	59.50	81.80	88.85	47.44
	DM-Adapter [29]	60.00	82.10	87.90	47.37
	FMFA (ours)	61.05	83.85	89.80	48.22
L	ACSA [32]	48.40	71.85	81.45	-
	CFine [53]	50.55	72.50	81.60	-
	PLOT [35]	61.80	82.85	89.45	-
	RaSa [2]	66.90	86.50	91.35	52.31
	APTM [55]	67.50	85.70	91.45	52.56
	<i>VL-Backbones with ReID-domain pre-training:</i>				
P+G	UniPT [41] + IRRA [21]	62.20	83.30	89.75	48.33
	PLIP [61] + IRRA [21]	64.35	83.75	91.00	50.93
	NAM [45] + IRRA ^R	68.25	86.75	92.30	52.92
	NAM [45] + FMFA (ours)	68.70	87.05	92.35	53.14
	HAM [22] + IRRA ^R	71.35	87.60	93.05	55.40
	HAM [22] + FMFA (ours)	71.80	88.05	93.15	55.72

the VL-Backbones with ReID-domain pre-training, our method achieves further gains, exceeding IRRA by 0.45% in Rank-1 with both the NAM-based and HAM-based backbones. Notably, FMFA achieves Rank-5 accuracy higher than 88% with the HAM-based backbone.

Evaluation Results on ICFG-PEDES. We assess FMFA on the ICFG-PEDES benchmark, with the results displayed in Table 5. Using VL-Backbones without ReID-domain pre-training, FMFA obtains the leading results across all metrics, attaining 64.29% Rank-1 and 39.43% mAP. Compared with

Table 5. Comparisons with state-of-the-art methods on the ICFG-PEDES dataset.

Type	Method	Rank-1	Rank-5	Rank-10	mAP
<i>VL-Backbones w/o ReID-domain pre-training:</i>					
G	Dual Path [59]	38.99	59.44	68.41	-
	IVT [43]	56.04	73.60	80.22	-
	CLIP [37]	56.74	75.72	82.26	31.84
	VGSG [17]	60.34	76.01	82.01	-
	DM-Adapter [29]	62.64	79.53	85.32	36.50
	IRRRA ^R [21]	63.48	80.16	85.78	38.20
	FMFA (ours)	64.29	80.48	85.93	39.43
L	SSAN [10]	54.23	72.63	79.53	-
	ISANet [54]	57.73	75.42	81.72	-
	CFine [53]	60.83	76.55	82.42	-
	RaSa [2]	65.28	80.40	85.12	41.29
	PLOT [35]	65.76	81.39	86.73	
<i>VL-Backbones with ReID-domain pre-training:</i>					
P+G	UniPT [41] + IRRRA [21]	64.50	80.24	85.74	38.22
	PLIP [61] + IRRRA [21]	65.79	81.94	87.32	39.43
	NAM [45] + IRRRA ^R	66.34	81.94	86.73	40.14
	NAM [45] + FMFA (ours)	66.58	81.94	87.04	40.17
	HAM [22] + IRRRA ^R	68.21	83.28	88.04	41.72
	HAM [22] + FMFA (ours)	68.37	83.28	88.10	41.76

IRRRA, FMFA shows a notable improvement of 0.81% Rank-1 and 1.23% mAP, which is meaningful for practical applications. When adopting VL-Backbones with ReID-domain pre-training, FMFA yields slight gains, outperforming IRRRA by 0.24% and 0.16% in Rank-1 with the NAM-based and HAM-based backbones, respectively.

In conclusion, FMFA attains the highest performance across all evaluation metrics on the three widely used public benchmarks. As far as we are aware, FMFA is the best method for all global matching methods. This highlights the ability of our method to generalize well and maintain robustness.

4.3 Ablation Study

In this subsection, we examine our proposed components in the FMFA framework. For simplicity, we omit the components of \mathcal{L}_{id} and the IRR module that were proposed by IRRRA and used in all experiments. Only one of SDM and A-SDM can be used at the same time.

To thoroughly assess the contribution of our FMFA modules, we undertake an empirical analysis on three widely used datasets. Table 6 summarizes the Rank-1/5/10 accuracies (%) together with the mAP (%) performance.

Effect of The A-SDM Module. To evaluate the contribution of the Adaptive Similarity Distribution Matching (A-SDM) module, we perform ablation experiments by replacing the A-SDM module with the SDM module, keeping all hyperparameters unchanged. Specifically, as shown in Table 6, replacing A-SDM with SDM results in a reduction of Rank-1 accuracy by 0.59%, 0.78%, and 0.75% across the three datasets, and also causes a 1.19% drop in mAP on the ICFG-PEDES dataset, as observed in No. 0 vs. No. 1. Additionally, all evaluation metrics on CUHK-PEDES and ICFG-PEDES degrade, further confirming the superiority of A-SDM. Moreover, when combined with the EFA module, the advantage of A-SDM becomes even more pronounced. As shown in No. 2 vs. No. 3, replacing the A-SDM module with the SDM module results in 0.43% and 0.48% decrease in Rank-1 and Rank-5 on the CUHK-PEDES dataset, respectively, as well as a 1.55% drop in Rank-5 and a 0.58% decline in mAP on the RSTPReid dataset. These results collectively validate the consistent and significant impact of A-SDM to performance.

Table 6. Ablation analysis of FMFA modules across three public benchmarks.

No.	Methods	Components			CUHK-PEDES				ICFG-PEDES				RSTPReid			
		SDM	A-SDM	EFA	Rank-1	Rank-5	Rank-10	mAP	Rank-1	Rank-5	Rank-10	mAP	Rank-1	Rank-5	Rank-10	mAP
0	Baseline	✓			73.45	89.38	93.69	66.13	63.48	80.16	85.78	38.20	59.50	81.80	88.85	47.44
1	+A-SDM		✓		74.04	89.86	93.89	66.45	64.26	80.59	85.90	39.39	60.25	81.45	88.70	47.69
2	+EFA	✓		✓	73.73	89.64	94.04	66.40	63.77	80.39	85.86	39.17	60.45	82.30	89.25	47.64
3	FMFA	✓	✓	✓	74.16	90.12	94.10	66.66	64.29	80.48	85.93	39.43	61.05	83.85	89.80	48.22

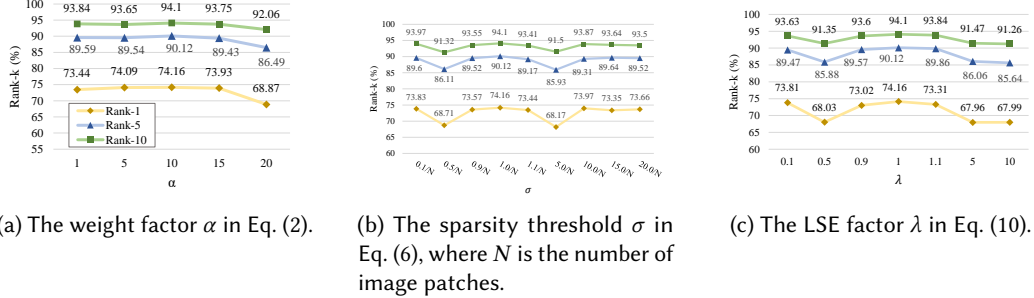


Fig. 4. The sensitivity analysis of hyperparameters of FMFA on the CUHK-PEDES dataset.

Effect of The EFA Module. To improve the model’s global matching performance, the Explicit Fine-grained Alignment (EFA) module introduces fine-grained cross-modal interaction based on a sparse similarity matrix. The impact of the EFA module is illustrated by comparing the results of No. 0 vs. No. 2 and No. 1 vs. No. 3. Specifically, as shown in No. 1 vs. No. 3, removing the EFA module from FMFA leads to a performance drop of 0.26% and 0.21% in Rank-5 and Rank-10 on the CUHK-PEDES dataset, and a more significant decline of 2.40% and 1.10% in Rank-5 and Rank-10, along with a 0.53% decrease in mAP on the RSTPReid dataset. However, EFA causes a 0.11% drop in Rank-5 on ICFG-PEDES, suggesting that its sparse and hard coding strategy, which focuses only on the most relevant patches, may overlook other informative ones and lead to information loss. Notably, this comparison also reflects the joint ablation of EFA and the A-SDM module, further verifying the complementary effect between the two modules. Moreover, to further validate the individual contribution of the EFA module, we design an additional experiment that retains the SDM module while removing only the EFA module, as observed in No. 0 vs. No. 2. In this setting, the absence of EFA results in 0.38%, 0.29%, and 0.95% drops in Rank-1 on CUHK-PEDES, ICFG-PEDES and RSTPReid, and causes a 1.23% drop in mAP on ICFG-PEDES. These evaluations highlight the effectiveness of the EFA module.

4.4 Parameter Study

We perform a parameter study on the CUHK-PEDES dataset, examining three hyperparameters—the weight factor α , the sparsity threshold σ , and the factor λ —as well as the contribution weights of the proposed loss functions, \mathcal{L}_{A-SDM} and \mathcal{L}_{EFA} . When examining a specific parameter, all other parameters are maintained as specified in Section 4.1.

Hyperparameters Analysis. As shown in Figure 4a, we vary the weight factor α from 1 to 20. The results on CUHK-PEDES show that setting α to 10 achieves the highest performance across the evaluated metrics, suggesting that the adaptive pull force on unmatched positive pairs is optimal. However, when α is increased to 20, the performance drops significantly because the pull force becomes excessively strong, causing unmatched positive pairs to fail to align properly and instead over-pulling mismatched positives, which leads to false positives. We further vary the sparsity

Table 7. The sensitivity analysis of the weight of \mathcal{L}_{A-sdm} and \mathcal{L}_{efa} on the CUHK-PEDES dataset, where one weight is varied and the other is fixed at 1.0.

Weight	\mathcal{L}_{A-sdm}			\mathcal{L}_{efa}		
	Rank-1	Rank-5	Rank-10	Rank-1	Rank-5	Rank-10
0.1	71.47	88.62	93.03	68.32	85.75	91.04
0.5	71.23	88.06	93.16	58.49	80.05	87.13
1.0	74.16	90.12	94.10	74.16	90.12	94.10
5.0	71.86	88.27	93.12	0.09	0.19	0.32
10.0	72.45	88.62	93.24	0.09	0.19	0.32

Table 8. Ablation study verifying the necessity of the constant term “+1” in A-SDM on the CUHK-PEDES dataset.

Setting	“+1” Term	Rank-1	Rank-5	Rank-10
A-SDM w/o “+1”		26.12	48.36	59.18
A-SDM w “+1”	✓	74.16	90.12	94.10

threshold σ from $0.1/N$ to $20/N$ and the LSE factor λ from 0.1 to 10, where N denotes the number of image patches. As illustrated in Figure 4b and Figure 4c, setting σ to $1/N$ and λ to 1 yields the best overall performance. When σ is set too high, only a few highly relevant patches are retained, leading to the loss of semantic information, whereas an excessively low σ preserves most patches and weakens the ability to capture discriminative features. According to Eq. (10), a large λ emphasizes the differences among patch responses and makes the pooling operation less robust to noise, while a small λ smooths these responses excessively and reduces feature discrimination. Moreover, to evaluate the stability of these hyperparameters, we further set σ around $1/N$ (i.e., $0.9/N$ and $1.1/N$) and λ around 1 (i.e., 0.9 and 1.1). The results show that although slightly adjusting σ and λ leads to a minor performance drop, our model still obtains high performance, demonstrating the robustness of our method.

Loss Function Weights. We perform experiments using the CUHK-PEDES dataset to investigate the influence of the weights of the two proposed loss functions, \mathcal{L}_{A-sdm} and \mathcal{L}_{efa} , varying them from 0.1 to 10.0, as shown in Table 7. To comprehensively explore the optimal combination of the proposed loss weights, we only vary one weight at a time while keeping the other fixed at 1 to ensure a controlled comparison. The results show that setting both weights to 1 yields the best performance. Notably, increasing the weight of \mathcal{L}_{efa} to 5.0 or 10.0 results in gradient explosion, making the model untrainable and causing all metrics to drop below 1.

The “+1” term in A-SDM. We carry out experiments on the CUHK-PEDES dataset to validate the necessity of the constant “+1” in A-SDM. As defined in Eq. (2), the constant term “+1” ensures a positive lower bound for the adaptive weight, preventing it from becoming zero when a pair is correctly matched. Without this term, gradients of correctly matched positive pairs diminish, leading to unstable optimization and degraded performance during training. Table 8 indicates that omitting the “+1” leads to a notable decline in retrieval accuracy, illustrating that the effectiveness of model is reduced. Therefore, the “+1” term is a crucial component that ensures stable optimization and consistent performance of A-SDM.

4.5 Qualitative Results

Visualization of The Sparse Process. We visualize the similarity maps before and after the sparse process (i.e., Eq. (5) and Eq. (6)) in the EFA module, as shown in Figure 5. Patches with high similarity (greater than 0.75) are preserved, as indicated by the black frames in the left part

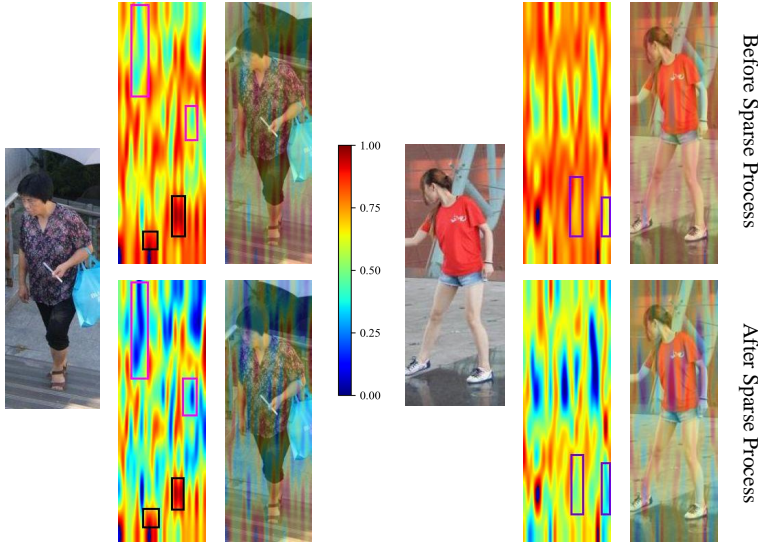


Fig. 5. Visualization of similarity maps before and after the sparse process in the EFA module.

of Figure 5. In contrast, patches with low similarity (below 0.5) are suppressed to values under 0.25 and thus omitted during aggregation, as shown by the pink frames on the left. When most patches in an image exhibit relatively high similarity (around 0.75), the sparse process retains only those with the highest similarity while reducing the similarity of the remaining patches below 0.5, highlighted by the purple frames in the right part of Figure 5. This guarantees that the subsequent aggregation emphasizes only the most pertinent patches, decreasing computational and memory overhead while preserving performance. Unlike implicit aggregation methods based on attention mechanisms, EFA explicitly aggregates image patches and text tokens, allowing us to observe whether the most relevant patches are effectively aggregated by visualizing the similarity between patches and tokens.

Inference Time Comparison. We compare the inference time between FMFA and recent matching methods (e.g., PLOT [35] and RaSa [2]) on the test sets of three datasets, as shown in Table 9. As a global matching method, FMFA only computes global features during inference, thus achieving a higher inference speed than local matching methods. Even when compared with the recent global matching method DM-Adapter [29], FMFA still achieves consistently faster inference across all three datasets. Moreover, the efficiency advantage of FMFA becomes more pronounced with the growth of the test set. For instance, the inference time of FMFA vs. PLOT increases from 3s vs. 5s on RSTPReid to 50s vs. 91s on ICFG-PEDES. These comparisons clearly demonstrate that FMFA achieves superior inference speed compared with recent methods.

Visualization of Top-5 Retrieval Results. Figure 6 compares the top-5 retrieval results between the baseline IRR^A and our proposed FMFA on the CUHK-PEDES dataset. Figure 6 illustrates that FMFA delivers more precise retrieval results, correctly identifying images that the baseline fails to match. For query texts where the baseline performs well, FMFA further improves performance by retrieving more relevant pedestrian images (e.g., Figure 6a and Figure 6c). Even for hard negative samples, where the baseline struggles to retrieve the correct image, FMFA still enhances the similarity between positive pairs (e.g., Figure 6b and Figure 6d). This is because our proposed

Table 9. Comparison of the inference time (s) between FMFA and recent methods.

Method	RSTPReid	CUHK-PEDES	ICFG-PEDES
FMFA (ours)	3	7	50
DM-Adapter [29]	8	16	78
PLOT [35]	5	16	91
APTM [55]	10	29	95
SCVD [51]	-	191	1369
RaSa [2]	388	1168	3871



Fig. 6. Top-5 retrieval results for each text query on CUHK-PEDES, comparing baseline with FMFA. Target image, correct matches, and mismatches are outlined in black, green, and red.

FMFA focuses on the unmatched positive pairs and adaptively pulls the positive pairs closer. More comparisons of the top-5 retrieved results are provided in Appendix B.

5 Conclusion

In summary, we propose a cross-modal Full-Mode Fine-grained Alignment (FMFA) framework to learn discriminative global text-image representations through full-mode fine-grained alignment, including explicit fine-grained alignment and existing implicit relational reasoning. We design an Adaptive Similarity Distribution Matching (A-SDM) module to concentrate on unmatched positive pairs, adaptively pulling them closer. In addition, to achieve cross-modal fine-grained alignment, we introduce an Explicit Fine-grained Alignment (EFA) module, which explicitly aggregates local

text and image representations based on the sparse similarity matrix and employs a hard coding method. These modules function together to project images and text into a shared embedding space. Comprehensive experiments across three datasets confirm the effectiveness and superior performance of our FMFA framework.

Limitation. The fixed threshold in the sparse process only keeps the most relevant patches, which may result in the loss of semantic information and limit the effective aggregation of local features, thereby affecting the overall performance of our model. Incorporating adaptive methods that capture complete semantic information (e.g., tree transformer [48]) could further enhance our model.

Acknowledgments

This work was supported by the National Natural Science Foundation of China (No. 62302080), Guangxi Key Research and Development Program (No. Guike AB24010112), National Foreign Expert Project of China (No. S20240327), Sichuan Science and Technology Program (No. 2025HJRC0021) and Sichuan Province Innovative Talent Funding Project for Postdoctoral Fellows (No. BX202312).

References

- [1] Jinze Bai, Shuai Bai, Shusheng Yang, Shijie Wang, Sinan Tan, Peng Wang, Junyang Lin, Chang Zhou, and Jingren Zhou. 2023. Qwen-VL: A Versatile Vision-Language Model for Understanding, Localization, Text Reading, and Beyond. *arXiv preprint arXiv:2308.12966* (2023).
- [2] Yang Bai, Min Cao, Daming Gao, Ziqiang Cao, Chen Chen, Zhenfeng Fan, Liqiang Nie, and Min Zhang. 2023. Rasa: Relation and sensitivity aware representation learning for text-based person search. In *Proceedings of the Thirty-Second International Joint Conference on Artificial Intelligence*. 555–563.
- [3] Ioana Bica, Anastasija Ilić, Matthias Bauer, Goker Erdogan, Matko Bošnjak, Christos Kapelanis, Alexey A Gritsenko, Matthias Minderer, Charles Blundell, Razvan Pascanu, and Jovana Mitrovic. 2024. Improving fine-grained understanding in image-text pre-training. In *Proceedings of the 41st International Conference on Machine Learning*. 3974–3995.
- [4] Min Cao, Yang Bai, Ziyin Zeng, Mang Ye, and Min Zhang. 2024. An empirical study of clip for text-based person search. In *Proceedings of the AAAI Conference on Artificial Intelligence*, Vol. 38. 465–473.
- [5] Yuxin Chen, Zongyang Ma, Ziqi Zhang, Zhongang Qi, Chunfeng Yuan, Bing Li, Junfu Pu, Ying Shan, Xiaojuan Qi, and Weiming Hu. 2024. How to Make Cross Encoder a Good Teacher for Efficient Image-Text Retrieval?. In *Proceedings of the IEEE/CVF Conference on Computer Vision and Pattern Recognition*. 26994–27003.
- [6] Yuxin Chen, Zongyang Ma, Ziqi Zhang, Zhongang Qi, Chunfeng Yuan, Ying Shan, Bing Li, Weiming Hu, Xiaohu Qie, and Jianping Wu. 2023. Vilem: Visual-language error modeling for image-text retrieval. In *Proceedings of the IEEE/CVF Conference on Computer Vision and Pattern Recognition*. 11018–11027.
- [7] De Cheng, Lingfeng He, Nannan Wang, Dingwen Zhang, and Xinbo Gao. 2025. Semantic-Aligned Learning with Collaborative Refinement for Unsupervised VI-ReID. *International Journal of Computer Vision* 133, 9 (2025), 5992–6014.
- [8] De Cheng, Jingyu Zhou, Nannan Wang, and Xinbo Gao. 2022. Hybrid Dynamic Contrast and Probability Distillation for Unsupervised Person Re-Id. *IEEE Transactions on Image Processing* 31 (2022), 3334–3346.
- [9] Jacob Devlin, Ming-Wei Chang, Kenton Lee, and Kristina Toutanova. 2019. Bert: Pre-training of deep bidirectional transformers for language understanding. In *Proceedings of the 2019 Conference of the North American Chapter of the Association for Computational Linguistics: Human Language Technologies, Volume 1 (Long and Short Papers)*. 4171–4186.
- [10] Zefeng Ding, Changxing Ding, Zhiyin Shao, and Dacheng Tao. 2021. Semantically self-aligned network for text-to-image part-aware person re-identification. *arXiv preprint arXiv:2107.12666* (2021).
- [11] Alex Ergastì, Tomaso Fontanini, Claudio Ferrari, Massimo Bertozzi, and Andrea Prati. 2025. MARS: Paying more attention to visual attributes for text-based person search. *ACM Transactions on Multimedia Computing, Communications, and Applications* 21, 10, Article 281 (2025), 22 pages.
- [12] Chenyang Gao, Guanyu Cai, Xinyang Jiang, Feng Zheng, Jun Zhang, Yifei Gong, Pai Peng, Xiaowei Guo, and Xing Sun. 2021. Contextual non-local alignment over full-scale representation for text-based person search. *arXiv preprint arXiv:2101.03036* (2021).
- [13] Xiao Han, Sen He, Li Zhang, and Tao Xiang. 2021. Text-based person search with limited data. *arXiv preprint arXiv:2110.10807* (2021).
- [14] Kaiming He, Xinlei Chen, Saining Xie, Yanghao Li, Piotr Dollár, and Ross Girshick. 2022. Masked autoencoders are scalable vision learners. In *Proceedings of the IEEE/CVF Conference on Computer Vision and Pattern Recognition*. 16000–16009.

[15] Kaiming He, Xiangyu Zhang, Shaoqing Ren, and Jian Sun. 2016. Deep residual learning for image recognition. In *Proceedings of the IEEE Conference on Computer Vision and Pattern Recognition*. 770–778.

[16] Lingfeng He, De Cheng, Nannan Wang, and Xinbo Gao. 2025. Exploring homogeneous and heterogeneous consistent label associations for unsupervised visible-infrared person reid. *International Journal of Computer Vision* 133, 6 (2025), 3129–3148.

[17] Shuting He, Hao Luo, Wei Jiang, Xudong Jiang, and Henghui Ding. 2024. VGSG: Vision-Guided Semantic-Group Network for Text-Based Person Search. *IEEE Transactions on Image Processing* 33 (2024), 163–176.

[18] David T. Hoffmann, Simon Schrödi, Jelena Bratulić, Nadine Behrmann, Volker Fischer, and Thomas Brox. 2024. Eureka-moments in transformers: multi-step tasks reveal softmax induced optimization problems. In *Proceedings of the 41st International Conference on Machine Learning*. 18409–18438.

[19] Shijuan Huang, Zongyi Li, Hefei Ling, and Jianbo Li. 2025. Cross-Modality Relation and Uncertainty Exploration for Text-Based Person Search. *ACM Transactions on Multimedia Computing, Communications, and Applications* 21, 12, Article 351 (2025), 20 pages.

[20] Zhong Ji, Junhua Hu, Deyin Liu, Lin Yuanbo Wu, and Ye Zhao. 2022. Asymmetric Cross-Scale Alignment for Text-Based Person Search. *IEEE Transactions on Multimedia* 25 (2022), 7699–7709.

[21] Ding Jiang and Mang Ye. 2023. Cross-modal implicit relation reasoning and aligning for text-to-image person retrieval. In *Proceedings of the IEEE/CVF Conference on Computer Vision and Pattern Recognition*. 2787–2797.

[22] Jiayu Jiang, Changxing Ding, Wentao Tan, Junhong Wang, Jin Tao, and Xiangmin Xu. 2025. Modeling Thousands of Human Annotators for Generalizable Text-to-Image Person Re-identification. In *Proceedings of the IEEE/CVF Conference on Computer Vision and Pattern Recognition*. 9220–9230.

[23] Kuang-Huei Lee, Xi Chen, Gang Hua, Houdong Hu, and Xiaodong He. 2018. Stacked cross attention for image-text matching. In *Proceedings of the European Conference on Computer Vision*. 201–216.

[24] Junnan Li, Dongxu Li, Silvio Savarese, and Steven Hoi. 2023. Blip-2: Bootstrapping language-image pre-training with frozen image encoders and large language models. In *Proceedings of the 40th International Conference on Machine Learning*. 19730–19742.

[25] Junnan Li, Dongxu Li, Caiming Xiong, and Steven Hoi. 2022. BLIP: Bootstrapping Language-Image Pre-training for Unified Vision-Language Understanding and Generation. In *Proceedings of the 39th International Conference on Machine Learning*. 12888–12900.

[26] Junnan Li, Ramprasaath Selvaraju, Akhilesh Gotmare, Shafiq Joty, Caiming Xiong, and Steven Chu Hong Hoi. 2021. Align before fuse: Vision and language representation learning with momentum distillation. *Advances in Neural Information Processing Systems* 34 (2021), 9694–9705.

[27] Shuang Li, Tong Xiao, Hongsheng Li, Bolei Zhou, Dayu Yue, and Xiaogang Wang. 2017. Person search with natural language description. In *Proceedings of the IEEE conference on Computer Vision and Pattern Recognition*. 1970–1979.

[28] Haotian Liu, Chunyuan Li, Yuheng Li, Bo Li, Yuanhan Zhang, Sheng Shen, and Yong Jae Lee. 2024. LLaVA-NeXT: Improved reasoning, OCR, and world knowledge. <https://llava-vl.github.io/blog/2024-01-30-llava-next/>

[29] Yating Liu, Zimo Liu, Xiangyuan Lan, Wenming Yang, Yaowei Li, and Qingmin Liao. 2025. Dm-adapter: Domain-aware mixture-of-adapters for text-based person retrieval. In *Proceedings of the AAAI Conference on Artificial Intelligence*. 5703–5711.

[30] Francesco Locatello, Dirk Weissenborn, Thomas Unterthiner, Aravindh Mahendran, Georg Heigold, Jakob Uszkoreit, Alexey Dosovitskiy, and Thomas Kipf. 2020. Object-centric learning with slot attention. *Advances in Neural Information Processing Systems* 33 (2020), 11525–11538.

[31] Jiasen Lu, Dhruv Batra, Devi Parikh, and Stefan Lee. 2019. Vilbert: Pretraining task-agnostic visiolinguistic representations for vision-and-language tasks. *Advances in Neural Information Processing Systems* 32 (2019), 13–23.

[32] Zefeng Lu, Ronghao Lin, Yap-Peng Tan, and Haifeng Hu. 2025. Prompt-guided Transformer and MLLM Interactive Learning for Text-Based Pedestrian Search. *IEEE Transactions on Information Forensics and Security* 20 (2025), 7181–7196.

[33] Jishnu Mukhoti, Tsung-Yu Lin, Omid Poursaeed, Rui Wang, Ashish Shah, Philip H. S. Torr, and Ser-Nam Lim. 2023. Open vocabulary semantic segmentation with patch aligned contrastive learning. In *Proceedings of the IEEE/CVF Conference on Computer Vision and Pattern Recognition*. 19413–19423.

[34] Aaron van den Oord, Yazhe Li, and Oriol Vinyals. 2018. Representation learning with contrastive predictive coding. *arXiv preprint arXiv:1807.03748* (2018).

[35] Jicheol Park, Dongwon Kim, Boseung Jeong, and Suha Kwak. 2024. PLOT: Text-Based Person Search with Part Slot Attention for Corresponding Part Discovery. In *Proceedings of the European Conference on Computer Vision*. 474–490.

[36] Yang Qin, Yingke Chen, Dezhong Peng, Xi Peng, Joey Tianyi Zhou, and Peng Hu. 2024. Noisy-correspondence learning for text-to-image person re-identification. In *Proceedings of the IEEE/CVF Conference on Computer Vision and Pattern Recognition*. 27197–27206.

[37] Alec Radford, Jong Wook Kim, Chris Hallacy, Aditya Ramesh, Gabriel Goh, Sandhini Agarwal, Girish Sastry, Amanda Askell, Pamela Mishkin, Jack Clark, Gretchen Krueger, and Ilya Sutskever. 2021. Learning transferable visual models

from natural language supervision. In *Proceedings of the 38th International Conference on Machine Learning*. 8748–8763.

[38] Robin Rombach, Andreas Blattmann, Dominik Lorenz, Patrick Esser, and Björn Ommer. 2022. High-Resolution Image Synthesis with Latent Diffusion Models. In *Proceedings of the IEEE/CVF Conference on Computer Vision and Pattern Recognition*. 10674–10685.

[39] Florian Schroff, Dmitry Kalenichenko, and James Philbin. 2015. Facenet: A unified embedding for face recognition and clustering. In *Proceedings of the IEEE conference on Computer Vision and Pattern Recognition*. 815–823.

[40] Rico Sennrich, Barry Haddow, and Alexandra Birch. 2016. Neural machine translation of rare words with subword units. In *Proceedings of the 54th Annual Meeting of the Association for Computational Linguistics (Volume 1: Long Papers)*. 1715–1725.

[41] Zhiyin Shao, Xinyu Zhang, Changxing Ding, Jian Wang, and Jingdong Wang. 2023. Unified Pre-training with Pseudo Texts for Text-To-Image Person Re-identification. In *Proceedings of the IEEE/CVF International Conference on Computer Vision*. 11140–11150.

[42] Zhiyin Shao, Xinyu Zhang, Meng Fang, Zhifeng Lin, Jian Wang, and Changxing Ding. 2022. Learning granularity-unified representations for text-to-image person re-identification. In *Proceedings of the 30th ACM International Conference on Multimedia*. 5566–5574.

[43] Xiujun Shu, Wei Wen, Haoqian Wu, Keyu Chen, Yiran Song, Ruizhi Qiao, Bo Ren, and Xiao Wang. 2022. See finer, see more: Implicit modality alignment for text-based person retrieval. In *Proceedings of the European Conference on Computer Vision*. 624–641.

[44] Naoya Sogi, Takashi Shibata, and Makoto Terao. 2024. Object-Aware Query Perturbation for Cross-Modal Image-Text Retrieval. In *Proceedings of the European Conference on Computer Vision*. 447–464.

[45] Wentao Tan, Changxing Ding, Jiayu Jiang, Fei Wang, Yibing Zhan, and Dapeng Tao. 2024. Harnessing the Power of MLLMs for Transferable Text-to-Image Person ReID. In *Proceedings of the IEEE/CVF Conference on Computer Vision and Pattern Recognition*. 17127–17137.

[46] Wilson L. Taylor. 1953. "Cloze procedure": A new tool for measuring readability. *Journalism Quarterly* 30, 4 (1953), 415–433.

[47] Bokun Wang, Yang Yang, Xing Xu, Alan Hanjalic, and Heng Tao Shen. 2017. Adversarial Cross-Modal Retrieval. In *Proceedings of the 25th ACM International Conference on Multimedia*. 154–162.

[48] Yaushian Wang, Hung-yi Lee, and Yun-Nung Chen. 2019. Tree Transformer: Integrating Tree Structures into Self-Attention. In *Proceedings of the 2019 Conference on Empirical Methods in Natural Language Processing and the 9th International Joint Conference on Natural Language Processing*. 1061–1070.

[49] Zhe Wang, Zhiyuan Fang, Jun Wang, and Yezhou Yang. 2020. Vitaa: Visual-textual attributes alignment in person search by natural language. In *Proceedings of the European Conference on Computer Vision*. 402–420.

[50] Zheng Wang, Zhenwei Gao, Yang Yang, Guoqing Wang, Chengbo Jiao, and Heng Tao Shen. 2025. Geometric Matching for Cross-Modal Retrieval. *IEEE Transactions on Neural Networks and Learning Systems* 36, 3 (2025), 5509–5521.

[51] Zhimin Wei, Zhipeng Zhang, Peng Wu, Ji Wang, Peng Wang, and Yanning Zhang. 2024. Fine-Granularity Alignment for Text-Based Person Retrieval Via Semantics-Centric Visual Division. *IEEE Transactions on Circuits and Systems for Video Technology* 34, 9 (2024), 8242–8252.

[52] Tinghui Wu, Shuhu Zhang, Dihu Chen, and Haifeng Hu. 2024. Text-and-Image Learning Transformer for Cross-Modal Person Re-Identification. *ACM Transactions on Multimedia Computing, Communications, and Applications* 21, 1, Article 27 (2024), 18 pages.

[53] Shuanglin Yan, Neng Dong, Liyan Zhang, and Jinhui Tang. 2023. Clip-driven fine-grained text-image person re-identification. *IEEE Transactions on Image Processing* 32 (2023), 6032–6046.

[54] Shuanglin Yan, Hao Tang, Liyan Zhang, and Jinhui Tang. 2023. Image-specific information suppression and implicit local alignment for text-based person search. *IEEE Transactions on Neural Networks and Learning Systems* 35, 12 (2023), 17973–17986.

[55] Shuyu Yang, Yinan Zhou, Zhedong Zheng, Yaxiong Wang, Li Zhu, and Yujiao Wu. 2023. Towards Unified Text-based Person Retrieval: A Large-scale Multi-Attribute and Language Search Benchmark. In *Proceedings of the 31st ACM International Conference on Multimedia*. 4492–4501.

[56] Xi Yang, Huanling liu, De Cheng, Nannan Wang, and Xinbo Gao. 2024. Feature-Level Adversarial Attacks and Ranking Disruption for Visible-Infrared Person Re-identification. *Advances in Neural Information Processing Systems* 37 (2024), 135043–135061.

[57] Lewei Yao, Runhui Huang, Lu Hou, Guansong Lu, Minzhe Niu, Hang Xu, Xiaodan Liang, Zhenguo Li, Xin Jiang, and Chunjing Xu. 2022. Filip: Fine-grained interactive language-image pre-training. In *International Conference on Learning Representations*.

[58] Ying Zhang and Huchuan Lu. 2018. Deep cross-modal projection learning for image-text matching. In *Proceedings of the European Conference on Computer Vision*. 686–701.

- [59] Zhedong Zheng, Liang Zheng, Michael Garrett, Yi Yang, Mingliang Xu, and Yi-Dong Shen. 2020. Dual-path convolutional image-text embeddings with instance loss. *ACM Transactions on Multimedia Computing, Communications, and Applications* 16, 2, Article 51 (2020), 23 pages.
- [60] Aichun Zhu, Zijie Wang, Yifeng Li, Xili Wan, Jing Jin, Tian Wang, Fangqiang Hu, and Gang Hua. 2021. Dssl: Deep surroundings-person separation learning for text-based person retrieval. In *Proceedings of the 29th ACM International Conference on Multimedia*. 209–217.
- [61] Jialong Zuo, Jiahao Hong, Feng Zhang, Changqian Yu, Hanyu Zhou, Changxin Gao, Nong Sang, and Jingdong Wang. 2024. PLIP: Language-Image Pre-training for Person Representation Learning. *Advances in Neural Information Processing Systems* 37 (2024), 45666–45702.

A Theoretical Analysis of Hard Coding in EFA

Given visual embeddings of an image $V \in \mathbb{R}^{N \times d}$ and its joint embeddings $E \in \mathbb{R}^{L \times d}$, where N is the number of image patches and L is the length of the joint embeddings, both the hard coding method and the soft coding method calculate the similarity matrix A to obtain the final similarity between V and E , which requires the same time complexity $O(NLd)$. When processing the similarity matrix A , our hard coding method calculates the maximum similarity for each row, which has a time complexity of $O(N)$, as described in Eq. (9) and Eq. (10). However, the soft coding method processes all similarities, resulting in a time complexity of $O(NL)$. Moreover, the spatial complexity of the hard coding method is $O(NL)$, which is significantly lower than the spatial complexity of the soft coding method, $O(Ld)$. This is based on the fact that $N \ll d$. Therefore, our hard coding method can effectively reduce the cost of training time and memory.

B More Comparisons of The Top-5 Retrieved Results

Figure 7 and Figure 8 show the comparisons of the top-5 retrieved results between the baseline and FMFA on the ICFG-PEDES and RSTPReid datasets, respectively. These comparisons further highlight the superiority and effectiveness of the proposed FMFA framework.

Received 15 August 2025; revised XX XXX 2025; accepted XX XXX 2025



Fig. 7. Top-5 retrieval results for each text query on ICFG-PEDES, comparing baseline with FMFA. Target image, correct matches, and mismatches are outlined in black, green, and red.



Fig. 8. Top-5 retrieval results for each text query on RSTPReid, comparing baseline with FMFA. Target image, correct matches, and mismatches are outlined in black, green, and red.